RESEARCH PAPER

Hydration and Engineering Properties of Mechanically-Activated Blended Cement from Processed Steel Slag and Limestone

Mojtaba Hosseini[1], Ali Allahverdi[2,*], Mohammad Jaafar Soltanian Fard[1,*]

* *ali.allahverdi@iust.ac.ir,*

[1] Department of Chemistry, Firoozabad Branch, Islamic Azad University, P.O. Box 74715-117, Firoozabad, Fars, Iran

[2] Cement Research Center, School of Chemical Engineering, Iran University of Science and Technology, Narmak 1684613114, Tehran, Iran

Received: January 2021 **Revised: June 2021** **Accepted: September 2021**

DOI: 10.22068/ijmse.2104

Abstract: *The present research work aims to evaluate the feasibility of processing and utilizing steel slag in binary and ternary cement blends with limestone. The physical and microstructural properties of binary and ternary blended cements produced by inter-grinding mixtures of ordinary Portland cement clinker, processed steel slag, and limestone in a laboratory ball mill with replacement levels varying from 0 wt.% to 30 wt.% were studied. The effects of processed steel slag and limestone incorporation on the density of dry cement mixes and water consistency, setting time, and volume stability of fresh and hardened cement pastes were investigated. Also, density, water absorption, total open pore volume (%), and compressive strength of cement mortars were measured. The mix with 15 wt.% limestone and 15 wt.% processed steel slag was selected as a typical ternary cement mix for complementary studies including X-ray diffractometry, thermal gravimetry, Fourier-transform infrared spectroscopy, and scanning electron microscopy analyses. The results show that removal of relatively high metallic content of steel slag increases its grindability for mechanical activation and improves its hydraulic properties effectively and makes it suitable for being recycled in the cement industry. The results show that mechanical activation of the cement mixes enhances the poor hydraulic activity of the processed steel slag and compensates for the strength loss to some extent. The physical and chemical properties of all studied blended cement mixes comply with ASTM standard specifications, except the compressive strength of the cement mixes at 28-days containing 20 wt.% or higher amounts of limestone ground to the relatively low Blaine specific surface area of about 3000 cm^2/g. All cement mixtures in all Blaine-specific surface areas had less compressive strength than plain cement.*

Keywords: *Ternary blended cement, Processed steel slag, Limestone, Mechanical activation.*

1. INTRODUCTION

Developing new blended types of cement has become an important topic among many researchers because of the environmental concerns and energy-efficiency matters. For such a purpose, it is possible to decrease the clinker content of cement and replace it with suitable supplementary cementing materials (SCMs). These materials are either natural resources such as natural pozzolans and limestone or by-products of industrial processes like fly ash, slags from metallurgical processes, silica fume, and rice husk ash [1].

Types of blended cement are standardized depending on the availability of the resources in different countries. Research activities in this field resulted in the development of several combinations considering the benefits of active SCMs and fillers to Portland cements that are well documented.

Since the 1990s, the production of blended cements made from Portland cement and two SCMs has been increased [2-5]. This type of cement is called ternary or blended cement and it has more advantages than some of the existing binary types [2-5]. Ternary blended cements comprising the blends of fly ash- silica fume or slag- silica fume are quite common and various studies have been conducted on these types of cement [2-6].

Slags are the by-product of the iron and steel industry, which is classified depending on the type of furnace from which it is produced. Steel slag and iron slag are the most important types of slag. The exact data on the annual global slag production is unavailable, but it is estimated to be around 330 and 240 million tons in 2018 for iron and steel slags, respectively [7]. Due to the fast growth of steel slag production (30 million tons globally in 2018 compared to 2017) [7-8], it is necessary to find a suitable way for recycling this

industrial waste and consequently decreasing its environmental effects.

In the production of blended cements, the use of steel slags such as basic oxygen furnace slag (BOFS), electric arc furnace slag (EAFS), and ladle furnace slag (LFS) is more limited compared to iron slags [9]. This is mainly due to the metallic iron content of steel slags, which make them difficult to grind in cement finish grinding operation. Limited studies are also devoted to the application of steel slags in cement and concrete industries [9-12]. According to these studies, steel slags can be used as raw material for partial replacement of cement kiln feed [10, 11], or as aggregate in cement-based materials [12], or even as SCMs for partial replacement of clinker in blended cements [9, 12].

In the cement industry, the production of each ton of clinker is the cause of the production of about 0.97 tons of carbon dioxide [13]. The goal of the cement industry is to reduce this amount by 50% in 2050 [10]. One of the primary paths toward reaching this goal is reducing the clinker content in cement. The use of steel slags as SCMs, therefore, can be of great interest in this context [14]. In addition, better understanding and utilization of steel slags are vital due to shortages in the conventional SCMs and for reducing waste landfilling.

Adding an optimum amount of limestone filler to the clinker completes the fine fraction of the granulometric curve of cement without any increase in the water demand of cement [1]. Moreover, it also improves the cement packing and blocks the capillary pores [1]. There are several reports on the positive influences of ground limestone as an SCM on microstructure and mechanical properties of concrete [15-20]. The existence of an optimum amount of limestone powder in Portland limestone cement paste increases the early compressive strength of cement due to its filling effect and also the formation of tricalcium aluminum carbonate hydrates [21]. An addition of 6 wt.% of limestone influences the hydration rate of the cement phases like C3S, C3A, and C4AF. This improves the early strength of the cement up to four days by providing more surfaces for nucleation and hydration products [20, 22]. Additionally, in ternary blended cements including slag and limestone together, the hydration of slag accelerates in the presence of limestone due to the aluminum dilution effect provided by adding limestone [21].

The current work devoted to the effects of processed steel slag and limestone incorporation on basic engineering properties of ternary blended cements is part of a research program for determining the mechanical and durability performance of ternary blended cements based on limestone and processed steel slag.

2. EXPERIMENTAL PROCEDURE

2.1. Materials

The used materials were ordinary Portland cement clinker provided by Sepehr cement company (Shiraz province, Iran), steel slag (SS) was provided by Esfahan steel company (Esfahan province, Iran), limestone (LS), and gypsum were prepared from quarries of Sepehr cement company. The chemical compositions of these materials are given in Table 1.

The following tests have been conducted for characterization of the SS:

Wet chemical analysis in accordance with ASTM C114

XRD patterns (Philips pw 1730)

Hydraulic activity with NaOH at different Blaine specific surface areas according to ASTM 1073.

2.2. Methods

2.2.1. Steel slag treatment

SS is usually difficult to grind due to its metallic (zero-valent) iron content. For this reason, utilization of SS is almost impossible in the cement industry.

Table 1. Chemical composition of materials

Raw material	Chemical composition (wt.%)								
	SiO_2	Al_2O_3	Fe_2O_3	CaO	MgO	SO_3	Na_2O	K_2O	LOI*
Clinker	21.10	5.79	3.11	65.36	1.50	0.81	0.14	0.71	0.80
Gypsum	8.10	0.52	0.34	29.09	0.34	38.00	-	-	19.10
Steel slag	13.78	7.48	21.17	45.08	4.8	0.33	-	-	5.70
Limestone	1.16	0.70	0.22	54.17	0.48	-	-	-	43.00

However, it can be processed through a multistep magnetic separation operation. Removing the metallic content of SS, not only increases its grindability for mechanical activation but also improves its hydraulic properties. The separated metallic pieces can also be recycled in the steel industry. In this research, the prepared SS was firstly processed magnetically in three consecutive steps. In the first step, the relatively big metallic pieces (larger than 100 mm) were separated using a big magnet. This step resulted in about 25 wt.% of weight loss, which is typically large. The second step was devoted to the separation of magnetic pieces smaller than 100 mm. In the second step, about 15 wt.% of the SS was separated as pieces exhibiting relatively strong magnetic properties due to their metallic iron content. Since some metallic iron parts are enclosed inside the SS particles, magnetic separation (the first and the second steps) cannot effectively separate these SS particles and a crushing operation to expose these metallic parts would be very helpful. The third magnetic separation step was therefore performed after crushing the SS to sizes smaller than 10 mm, which resulted in the separation of about 10 wt.% of SS. All the three steps performed manually together resulted in a separation of about 43 wt.% of the SS as high metallic content part. The processed SS (PSS) was then used in this research work. Table 2 displays the chemical composition of the SS after each separation stage.

2.2.2. Cement mixes preparation

Various ternary cement blends with different proportions have been studied and they are given in Table 3. PSS and LS were added as partial cement replacements at different weight levels. Then, the ternary cement combinations were inter-ground in a laboratory ball mill (diameter 50 cm; length 50 cm; steel balls weight 100 kg) into four dissimilar Blaine with the specific surface areas of approximately 3000, 3500, 4000, and 4500 cm^2/g. By doing so, 32 different ternary mixes of blended cements were obtained for additional analysis.

The prepared mixes have been characterized by performing the following tests depending on their type:

For the dry mixes of cements, the residue of sieves 45 and 90 µm (wt. %) and the density have been obtained. Moreover, the Blaine specific surface area has been measured according to the ASTM C204 standard. Water consistency test (wt.%) and setting time (min) in accordance with ASTM C187 and ASTM C191, for the fresh cement pastes, have been obtained. X-ray diffractometry and scanning electron microscopy have been performed for the hardened cement pastes. The water absorption, total open pore volume, and density of the hardened cements (wt.%) were measured following ASTM C642. For this purpose, cylindrical mortar specimens have been used. Moreover, compressive strengths after 1, 3, 7, 28, and 56 days of curing in lime-saturated water were measured per ASTM C348 and C349.

3. RESULTS AND DISCUSSION

3.1. Materials

3.1.1. Chemical composition

As seen in Tables 1 and 2, the main oxides of the SS and PSS include CaO, followed by SiO_2, Fe_2O_3, Al_2O_3, and MgO. The chemical composition can provide some information about the basicity of SS and PSS. The $(CaO + MgO + Al_2O_3)/SiO_2$ ratio is more than 1 (4.16 and 3.60 for SS and PSS, respectively) providing basic character for the PSS and suggesting that this PSS may have proper latent hydraulic activity.

Table 2. Chemical composition of the steel slag after each separation stages

Steel slag	Chemical composition (wt.%)					
	SiO_2	Al_2O_3	Fe_2O_3	CaO	MgO	SO_3
Step 1	13.78	7.48	21.17	45.08	4.80	0.33
Step 2	15.50	7.93	14.85	47.74	5.20	0.37
Step 3	16.00	7.73	11.54	44.93	4.93	0.38

Table 3. Mix proportions (wt.%, to the total mix weight)

Clinker + Gypsum*	100	70	70	70	70	70	70	70
Steel slag	0	30	25	20	15	10	5	0
Limestone	0	0	5	10	15	20	25	30

3.1.2. *Hydraulic properties*

Table 4 shows the hydraulic activity of PSS determined in accordance with ASTM C1073 at different Blaine-specific surface areas.

As seen, increasing the Blaine specific surface areas of the PSS from 3000 cm^2/g to 4500 cm^2/g by mechanical activation increases its hydraulic activity by about 60%. Although mechanically activated steel slag exhibits a significantly higher hydraulic activity, its activity is still remarkably lower than that of granulated blast furnace slag [23].

Table 4. Hydraulic activity of processed steel slag at different Blaine specific surface areas according to ASTM C1073.

Blaine specific surface area (cm^2/g)	Time of hardening (hours)	Compressive strength (MPa)
3000	24	2.2
3500	24	2.6
4000	24	3.0
4500	24	3.5

3.1.3. *Mineralogical phase compositions*

Fig. 1 displays the XRD patterns of PSS and LS. It shows that major phases of PSS are the portlandite ($Ca(OH)_2$), magnetite (Fe_3O_4), and RO (CaO - MgO - FeO - MnO solid solution) phase. Small amounts of crystalline calcium silicates (C_3S and C_2S) are also present in the PSS. The hump at around 2-theta of 35˚ is an indication of the presence of amorphous silicate and/or aluminosilicate as reported in almost all of the water-cooled slags. The presence of portlandite in this basic SS also confirms that this SS was produced recently and there was no time for conversion of portlandite to calcite due to atmospheric carbonation. However, the crystalline content of this SS that is relatively high shows that the slag was not well quenched and was cooled slowly. Silicate phases of the SS either crystalline or amorphous are responsible for its latent hydraulic properties. The solid solution phase mentioned in Fig. 1 has a standard X-ray-card. Since the slag is a by-product of the steel industry, depending on the type and quality of raw materials, the composition of slag is different and as a result, will give a different range. To prevent excessive congestion, the characteristic peaks of phases such as merwinite, bredigite, cuspidine, and periclase are not specified. All of the peaks of the LS diffraction pattern belong to calcite.

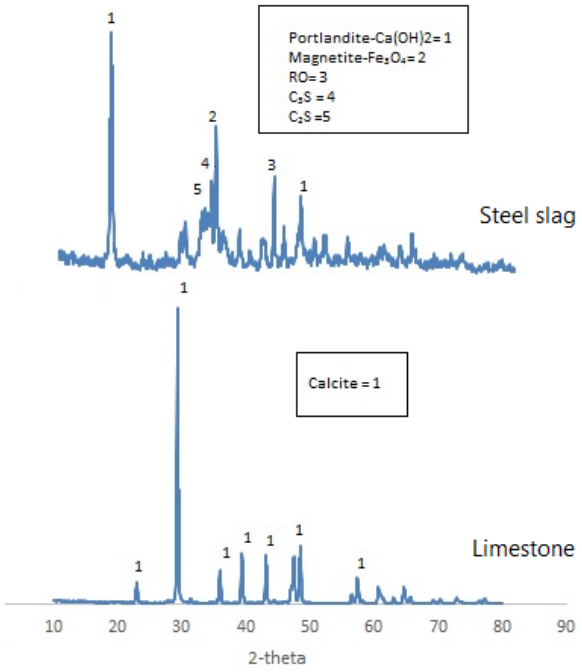

Fig. 1. XRD patterns of processed steel slag and limestone.

Table 5 represents the Bogue's potential phase composition of the used ordinary Portland cement clinker.

Table 5. Bogue's potential phase composition of ordinary Portland cement clinker.

Phase	C_3S	C_2S	C_3A	C_4AF
wt.%	60.37	15.2	10.08	9.45

3.2. Dry cement mixes

3.2.1. *Fineness*

The fineness of the cements can change the hydration rate noticeably. As a consequence, the rate of strength gain and heat evolution will be affected by this parameter, particularly at early ages. A common approach among many cement factories for controlling this parameter is by measuring both Blaine-specific surface areas and residue on 45 and/or 90 µm sieves. Figs. 2 and 3 represents the variation of residues of sieves 45 and 90 µm by replacement levels of SS(LS) in wt.%(wt. %) at various Blaine-specific surface areas.

Evidently, mixes with higher Blaine-specific surface areas have lower amounts of residue. Compared to plain cements, all mixes exhibit higher amounts of residue. The mix with 30%

PSS and 0% LS shows higher residues compared to plain cements due to the hardness of PSS (grindability about 16 kWh/t by work bond mill) compared to clinker (grindability about 14 kWh/t by work bond mill). As seen, incorporation of LS increases the residues. The higher the LS incorporation level, the higher the residues. LS (grindability about 11 kWh/t by work bond mill) exhibits a considerably lower hardness compared to PSS and clinker. When a relatively soft material like LS is inter-ground with a relatively hard material like clinker or PSS, it is easily crushed into the fine fraction resulting in relatively high Blaine specific surface areas while the hard component of the mix is not yet enough crushed resulting in a relatively higher coarse fraction [22]. The higher the proportion of the LS, the higher the coarse fraction of the residue on a sieve.

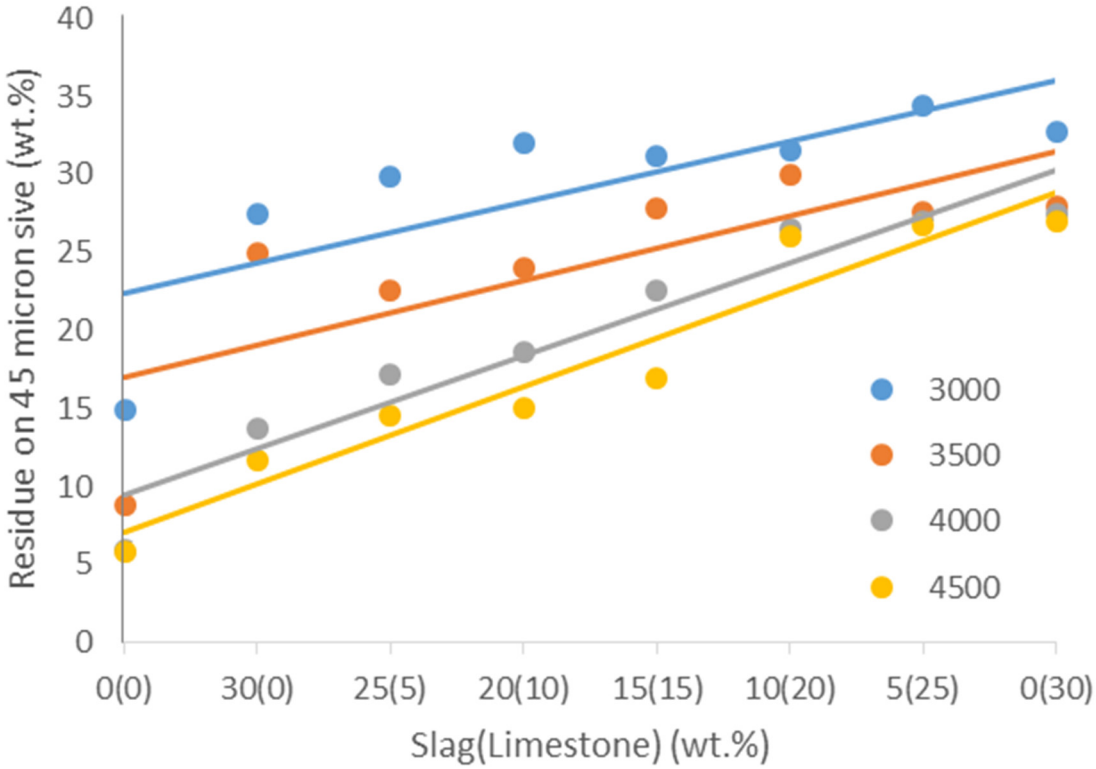

Fig. 2. Residues on 45 µm sieve versus processed steel slag and limestone (wt.%) at various Blaine specific surface areas.

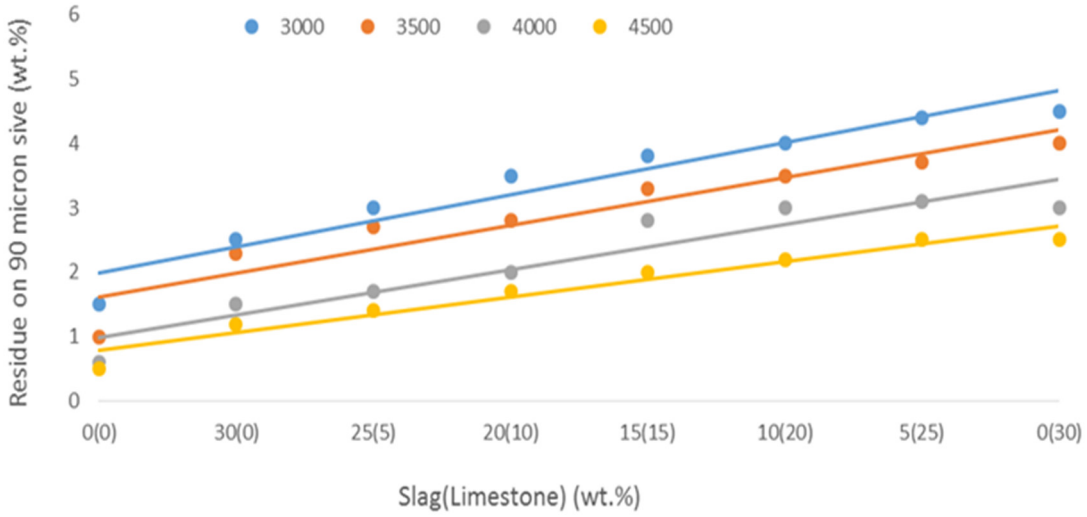

Fig. 3. Residues on 90 µm sieve versus processed steel slag and limestone (wt.%) at various special areas.

3.2.2. *Density*

Another significant parameter is the density of the cement. Density shows its importance in the calculation of concrete blends proportioning. The effect of PSS and LS on the cement's density is presented in Fig. 4. As seen, the mix incorporating 30% PSS and 0% LS exhibits the highest density (3.18 g/cm^3), and the mix with 30% LS and 0% PSS has the lowest density (2.97 g/cm^3). This is due to the fact that compared to plain cement with a density of 3.12 g/cm^3, PSS and LS with densities of 3.3 g/cm^3 and 2.8 g/cm^3 are more and less dense materials, respectively. The differences in densities originate from the chemical composition. Compared to plain cement, PSS has a much higher content of iron oxide with a high molecular weight (159.69 g/mol), whereas LS is mainly composed of calcium oxide with a relatively low molecular weight (56.08 g/mol).

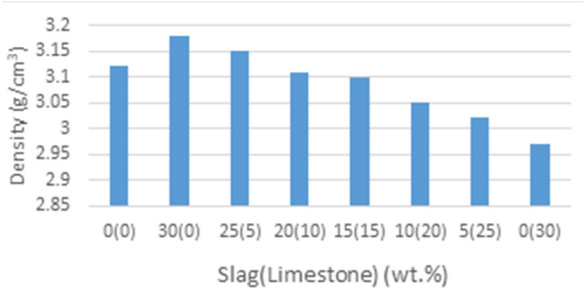

Fig. 4. Density versus processed steel slag and limestone (wt.%)

3.3. Fresh cement pastes

3.3.1. *Water consistency*

The flowability or comparative mobility of a fresh cement mix can be shown by water consistency. Fig. 5 shows the effect of the water-to-cement ratio for normal consistency on PSS and LS contents at several Blaine-specific surface areas. Both PSS and LS reduce the required water to have a normal consistency.

The required water for normal consistency depends on the fineness of the mix, the water demand of each component of the mix is influenced by its microstructure (porosity) and the shape of its particles.

An increase in the fineness increases the surface area to be wetted and results in higher water demand for normal consistency (as seen in Fig. 4). The microstructure of the material is also very important. Materials with porous microstructures adsorb more water inside their pore volumes in addition to their external surfaces. Compared to Portland cement clinker, PSS and LS are both among the materials of less porous microstructure [24, 25]. In addition, LS is believed to impart a plasticizing effect in cement mixes [26]. LS fine particles with a relatively lower tendency for water adsorption fill in the spaces between the larger clinker and PSS particles and impart a plasticizing effect reducing the water demand.

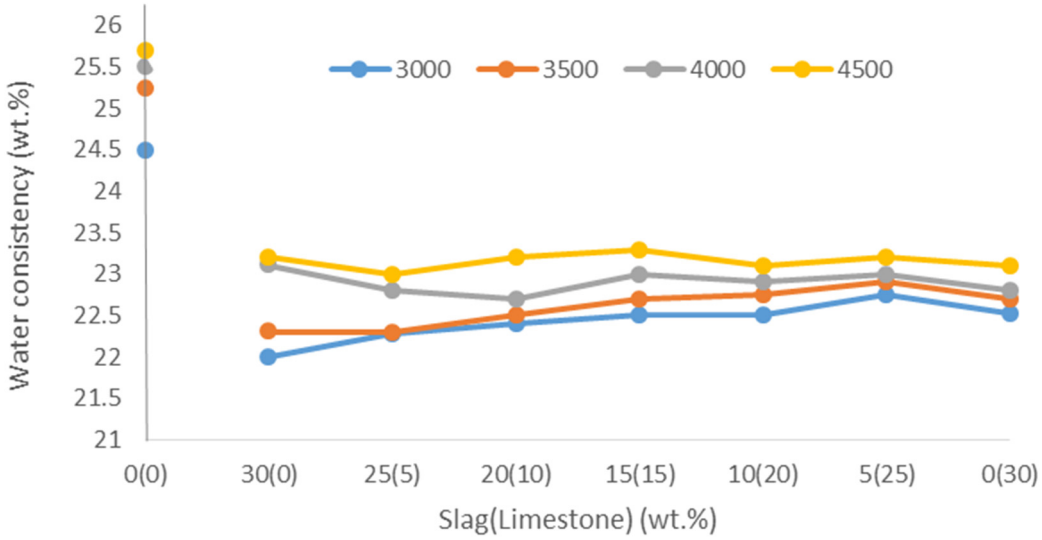

Fig. 5. Variations in normal water consistency of mixes versus processed steel slag and limestone (wt.%) at various Blaine specific surface areas.

3.3.2. *Setting times*

The hardening behavior of the cement pastes is described by setting times. Figs. 6 and 7, show initial and final setting times of the cement mixes, respectively. As seen, replacement of clinker with PSS in the mix incorporating 30% PSS and 0% LS increased both initial and final setting times confirming the less reactivity and the very slow hydration reactions of PSS compared to Portland cement [27].

The incorporation of LS as a replacement of PSS, however, results in more increases in both setting times showing that LS is even less reactive than PSS. LS is not completely inert in cementitious materials as it can react with aluminates of the clinker such as C_3A to produce carboaluminate hydrates [19, 20]. Although the formation of carboaluminate hydrates by reducing the concentration of C_3A can slightly increase the setting time, the main reason for setting time elongation is the dilution caused by high levels of replacement. The decrease of setting times was also observed with increasing Blaine-specific surface area that enhances the chemical reactivity of the components. All the obtained values of initial and final setting time tests are in accordance with ASTM C150.

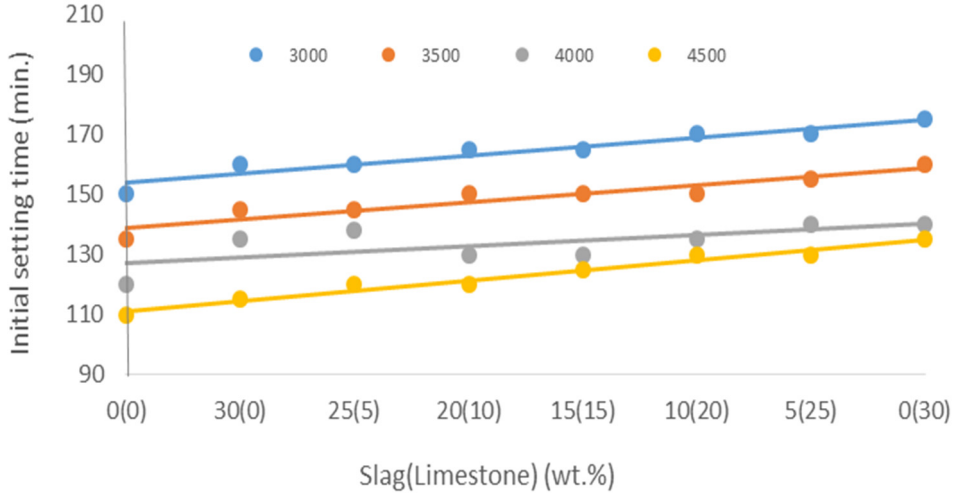

Fig. 6. Initial setting times versus processed steel slag and limestone (wt.%) at various Blaine specific surface area.

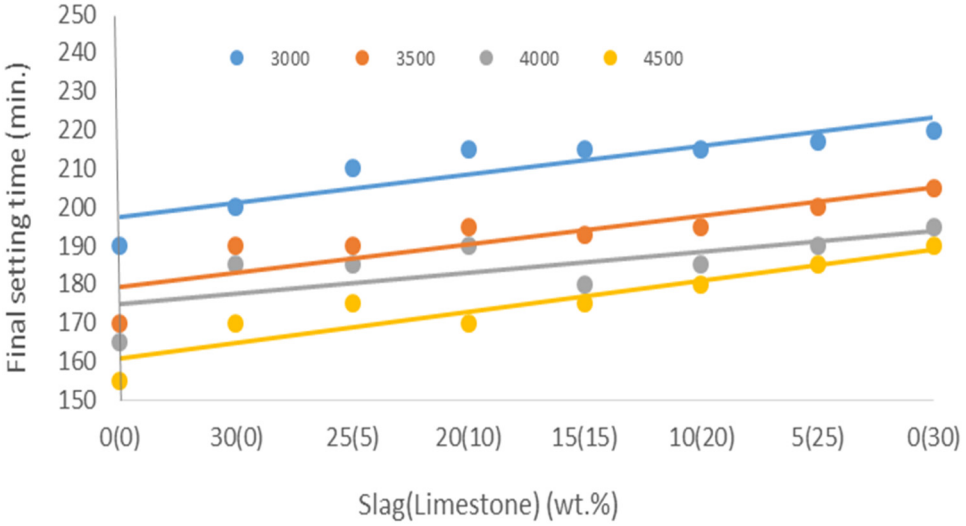

Fig. 7. Final setting times versus processed steel slag and limestone (wt.%) at various Blaine specific surface area.

3.4. Hardened cement mortars

3.4.1. Compressive strength

Fig. 8 represents the results obtained from compressive strength measurements. Each result is the average of three tests for each sample. As seen, the compressive strength increased considerably by increasing Blaine-specific surface area in all mixes of the same composition. Substitution of cement clinker with both LS and PSS reduced compressive strength in all ages. As expected, the effect of LS in strength loss, however, is more remarkable. PSS exhibits a weak latent hydraulic property that can be effectively enhanced by mechanical activation. LS substitution up to 20 wt.% causes the 28-day compressive strength at the lowest Blaine-specific surface area (3000 cm^2/g), that approaching the standard limit of 32.5 MPa. Mechanical activation, however, effectively increases the compressive strength.

As can be seen in the mix incorporating 25 wt.% PSS and 5 wt.% LS, it seems that relatively small incorporation of LS (up to 5 wt.%) into the ternary cement mix can slightly enhance the 56-day compressive strength at relatively higher Blaine specific surface areas (higher than 3500 cm^2/g), compared to the mix incorporating 30 wt.% PSS and 0 wt.% LS. This is due to the filling effect of the LS resulting in a more compact microstructure in the hardened cement mortar [1]. Another reason is that the Calcite present in limestone reacts with alumina to form hemi- and hemi- and monocarboaluminate phases. This results in the stabilization of ettringite, thus reducing porosity and increasing compressive strength. This effect is noticeable in low percentages of limestone. In this study, the highest compressive strength is related to the mixture of 5% LSS.

3.4.2. Water absorption, total open pore volume and density

Figs. 9 to 11 represent the changes in density, total open pore volume, and water absorption of 56-day cured mortar specimens at various Blaine-specific surface areas, respectively. As seen, mechanical activation and, especially replacement level can result in considerable changes in these properties. Mortar density increases with mechanical activation. This is not only due to the better packing of the particles at higher Blaine-specific surface areas but also due to the achievement of a higher degree of hydration at higher Blaine-specific surface areas. In fact, increasing Blaine-specific surface areas, packing density and a higher degree of hydration together result in the formation of a less porous and more compact microstructure [28].

As seen in Figs. 10 and 11, both water absorption and total open pore volume increase by about 10 to 15% with 30 wt.% replacement of clinker with PSS. Also, with the gradual replacement of PSS with LS, a very small increase in water absorption and total open pore volume are observed. Both PSS and LS result in slightly increased water absorption and total open pore volume due to their less or non-reactivity compared to Portland cement clinker. The non-reactivity of the LS, however, to some extent is compensated by its filling effect. As expected, any increase in Blaine-specific surface areas leads to microstructural condensation and acceleration of hydration reactions through the effect of mechanical activity. This in turn can positively affect the water absorption and open-pore volume.

3.5. Supplemental studies

As seen in the preceding parts, given the relatively low hydraulic latent property of PSS and almost non-reactivity of LS, all physical and chemical characteristics of the studied blended cement mixes comply with ASTM standard specifications, except the 28-day compressive strength of cement mixes containing 20 wt.% or higher amounts of LS ground to the relatively low Blaine specific surface area of 3000 cm^2/g. It is also observed that mechanical activation can effectively reduce the loss of compressive strength at relatively high replacement rates of LS. Nonetheless increasing the actual surface area of Blaine by mechanical activation results in considerably higher production costs by raising the rate of energy consumption in the cement mill and therefore relatively high replacement rates may not be technically sufficient. Given that PSS is a hard component, it is harder to grind it than LS. Different criteria including cement properties and economic benefits should be considered for the selection of the optimum blend. Economic considerations involve LS and SS availability and costs for cement plant and energy consumption in the cement mill to grind PSS. Knowing that incorporation of slag may enhance some durability properties of cement-like sulfate resistance [29, 30], some of the studied blends

may exhibit higher sulfate resistance compared to the control cement. In this case, durability properties can also be considered for the selection of the optimum blend. Here for complementary studies, a typical blend with relatively moderate replacement levels (15 wt.% LS and 15 wt.% PSS) ground to the Blaine specific surface area of 3500 cm2/g has been selected. To investigate the effects of both PSS and LS on cement properties, three control mixes including the binary mix containing 30 wt.% PSS, the binary mix containing 30 wt.% LS, and the plain Portland cement, all ground to the Blaine specific surface area of 3500 cm^2/g were are also considered.

All the complementary studies were performed on 84-day cured pastes of the selected ternary blend as well as the three control mixes.

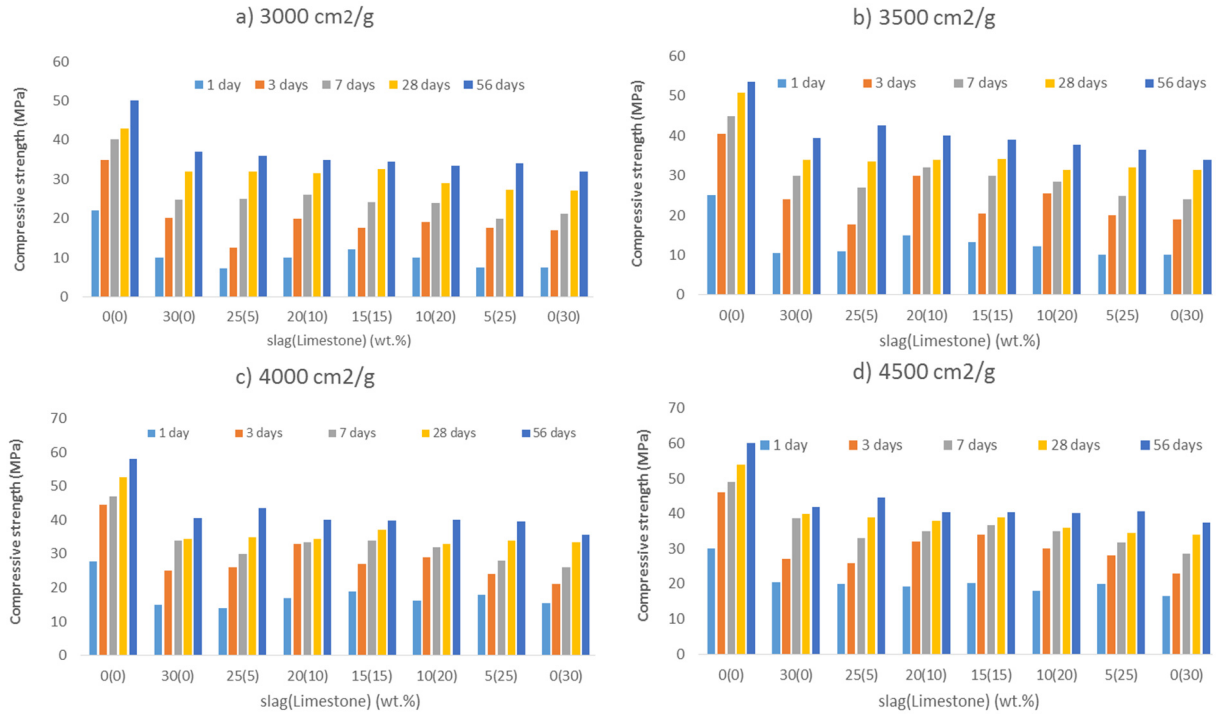

Fig. 8. Compressive strength versus processed steel slag and limestone (wt.%) at various Blaine specific surface areas.

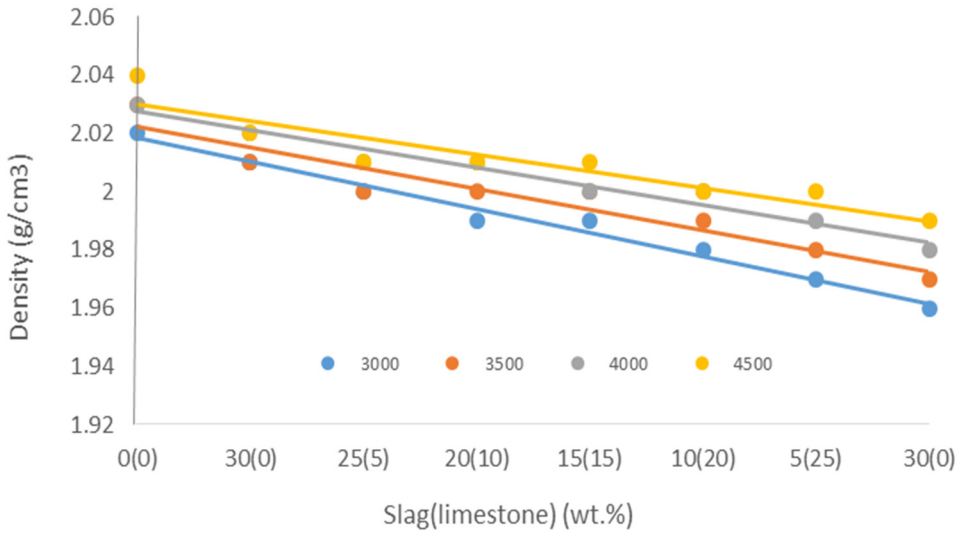

Fig. 9. Density versus processed steel slag and limestone (wt.%) at various Blaine specific surface areas.

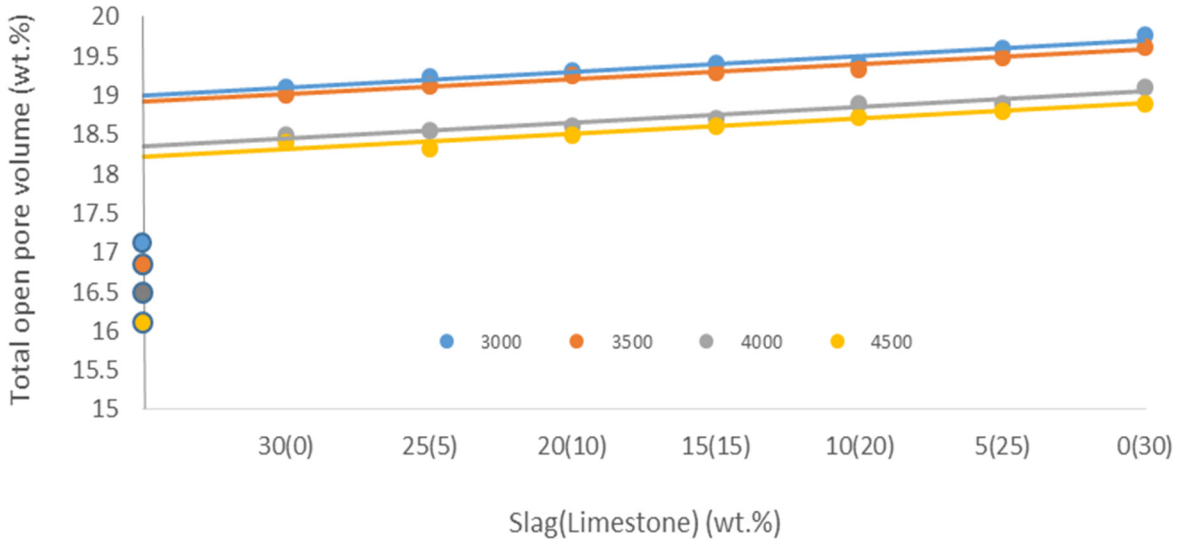

Fig. 10. Total open pore volume versus processed steel slag and limestone (wt.%) at various Blaine specific surface areas

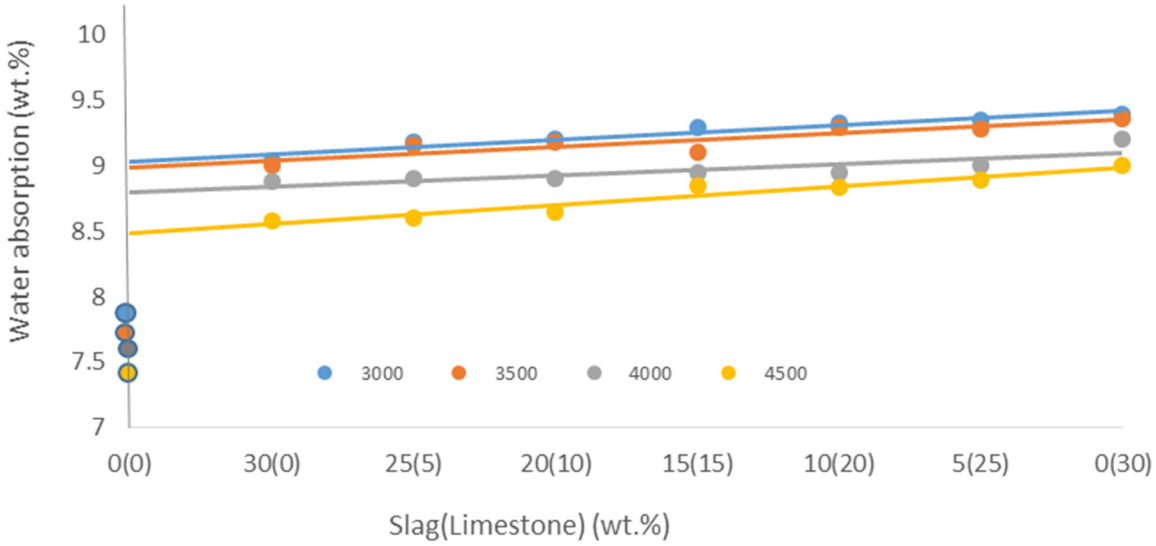

Fig. 11. Water absorption versus processed steel slag and limestone (wt.%) at various Blaine specific surface areas.

3.5.1. X-ray diffraction patterns

The X-ray diffraction patterns obtained from 84-day cured paste of selected ternary cement mix possessing 15 wt.% LS and 15 wt.% PSS along with 84-day cured pastes of plain Portland cement, a mix containing 30 wt.% PSS, and mix containing 30 wt.% LS as controls, all ground to the Blaine specific surface area of 3500 cm^2/g are represented in Fig. 12.

Fig. 12. X-ray diffraction patterns of 84-day cured paste of the selected ternary cement mix containing 15 wt.% limestones and 15 wt.% processed steel slag 15(15), along with 84-day cured pastes of plain Portland cement 0(0), a mix containing 30 wt.% steel slag 30(0), and mix containing 30 wt.% limestones as controls 0(30)

As seen, all the 84-days cured cement samples contained the same four crystalline phases including; portlandite, calcite, alite, and belite. There is no sign of ettringite showing full conversion of which into monosulfate after 84 days of curing. All hydration products are amorphous except portlandite. The presence of significant amounts of alite and belite phases in the plain Portland cement after 84 days of curing is a sign of the presence of relatively large alite and belite crystals in the used Portland cement clinker.

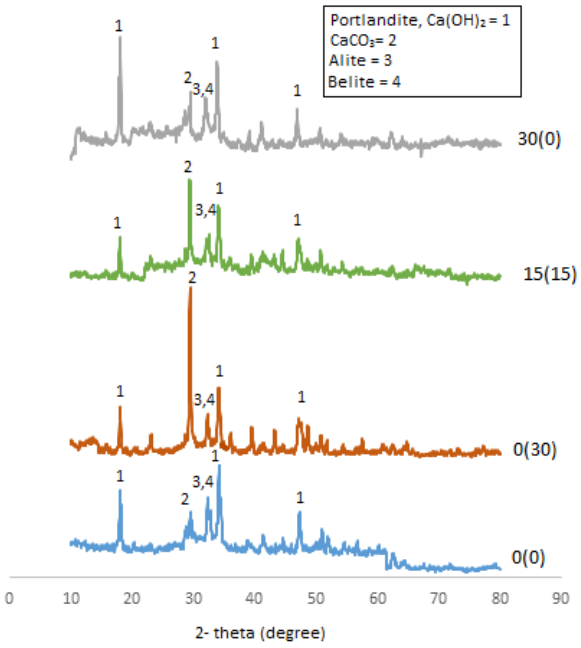

Fig. 12. X-ray diffraction patterns of 84-day cured paste of the selected ternary cement mix containing 15 wt.% limestones and 15 wt.% processed steel slag 15(15), along with 84-day cured pastes of plain Portland cement 0(0), a mix containing 30 wt.% steel slag 30(0), and mix containing 30 wt.% limestones as controls 0(30).

The amount of alite and belite phases were reduced in all binary and ternary blended cement mixes especially those containing 15 wt.% and 30 wt.% LS. This is mainly due to the dilution effect and probably partly due to the hydration acceleration caused by very fine LS particles providing nucleation sites for hydration products of alite and belite [20]. Since the portlandite phase originated from both PSS and also as a hydration product of alite and belite phases in the clinker, the diffraction pattern of the binary blended cement containing 30 wt.% PSS shows the highest intensity in portlandite peak. The formation of calcite in the plain Portland cement is a sign of partial atmospheric carbonation of the portlandite phase after relatively long water curing regime of 84 days. Because of the amorphous character of C-S-H, as the main binding compound and the common hydration product of both clinker and PSS, X-ray diffraction patterns results were not useful in characterizing the contribution of PSS in the hydration reactions and therefore other useful laboratory techniques including TGA and FTIR spectroscopy were considered.

3.5.2. Thermal analysis

The results of TGA measurements performed on the 84-day cured paste of the selected cement mix containing 15 wt.% LS and 15 wt.% PSS and 84-day cured pastes of control cement mixes including; the mix containing 30 wt.% PSS, the mix containing 30 wt.% LS, and the plain Portland cement, all ground to the Blaine specific surface areas of 3500 cm^2/g, are shown in Fig. 13.

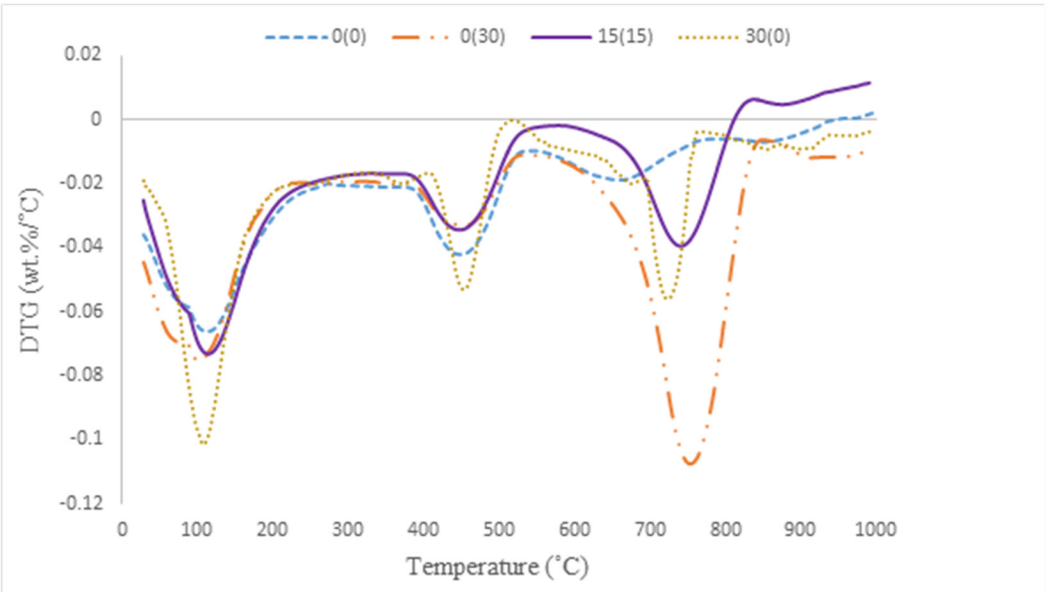

Fig. 13. DTG curves of 84-day cured paste of the selected ternary cement mix containing 15 wt.% limestone and 15 wt.% processed steel slag 15(15), along with 84-day cured pastes of plain Portland cement 0(0), mix containing 30 wt.% processed steel slag 30(0), and mix containing 30 wt.% limestone as controls 0(30).

As seen, the derivative thermal gravimetry (DTG) curves show the existence of some endothermic effects at about 110˚C, 450˚C, and 750˚C. Mass loss up to 300˚C corresponds to water loss of different hydrated phases of calcium silicate and calcium aluminate formed in cement pastes [31]. As can be seen, the smallest and the biggest dehydration effects appeared at about 110˚C belong to the plain Portland and the binary cement mix containing 30 wt.% PSS, respectively, clarifying the contribution of PSS in hydration reactions. The endothermic effects at about 450˚C are caused by the decomposition of portlandite [32], while the endothermic effects in the temperature range of 700-850˚C originate from the decomposition of calcium carbonate [33]. The strongest endothermic dehydroxylation (at about 450˚C) and decarbonisation (in the range 700-850˚C) effects belong to the binary mixes containing 30 wt.% PSS and 30 wt.% LS that contained the highest amounts of portlandite and calcite, respectively.

3.5.3. FTIR- spectroscopy

Fig. 14 shows the FTIR spectra of the 84-day cured paste of the selected ternary cement mix containing 15 wt.% LS and 15 wt.% PSS, along with 84-day cured pastes of control mixes including the mix containing 30 wt.% PSS, the mix containing 30 wt.% LS, and the plain Portland cement, all ground to the Blaine specific surface areas of 3500 cm^2/g. The bands appearing in the wavenumbers ranging from 970 cm^{-1} to about 1100 cm^{-1} correspond to C-S-H formation [34]. Also, the pattern of the spectrum in the 800-1100 cm^{-1} region is a characteristic of the asymmetric stretching vibration associated with the Si–O bonds in C-S-H gel Q2 units [35]. A shift in the Si–O stretching vibration to a higher wavenumber can be attributed to fingerprint evidence of the polymerization due to C-S-H gel hydration. As seen, the C-S-H stretching vibration band appeared at about 971 cm^{-1} for both the selected cement mix containing 15 wt.% PSS and 15 wt.% LS and also for the binary cement mix containing 30 wt.% LS, whereas for plain Portland cement and the binary cement mix containing 30 wt.% PSS, this band appeared at higher wavenumbers of about 975 cm^{-1} and 984 cm^{-1}, respectively, confirming the effect of PSS in the polymerization of C-S-H gel.

The sharp band at 3646 cm^{-1} belongs to the OH stretching vibration in portlandite [36, 37], and as seen, the highest and the lowest intensity for this band belong to the binary cement mix with 30 wt.% PSS and the control plain Portland cement, respectively, as observed previously in XRD and DTG results. The absorption band observed at 1418 cm^{-1} as well as those that appeared at 875 cm^{-1} and 712 cm^{-1} refer to the existence of $CO3^{-2}$ in the mixes [38, 39]. The broadband near 2900–3550 cm^{-1} and the band at 1640 cm^{-1} correspond to stretching [38] and bending of H_2O [40], respectively.

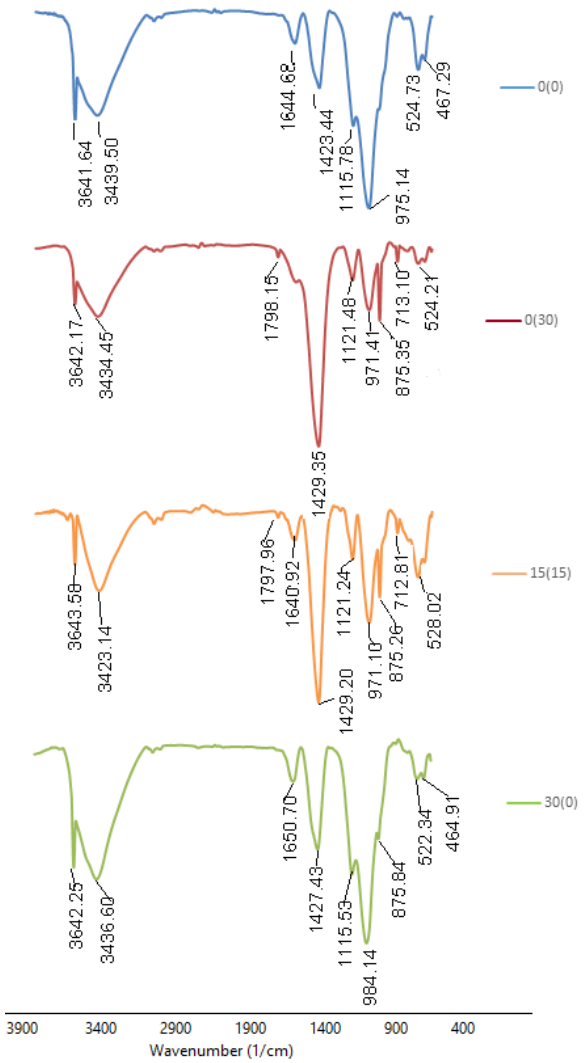

Fig. 14. FTIR spectra of 84-day cured paste of the selected ternary cement mix containing 15 wt.% limestones and 15 wt.% processed steel slag 15(15), along with 84-day cured pastes of plain Portland cement 0(0), a mix containing 30 wt.% processed steel slag 30(0), and mix containing 30 wt.% limestones as controls 0(30).

3.5.4. *Microstructural studies*

Fig. 15 shows a typical SEM image of the 84-day cured paste of the selected ternary cement mix containing 15 wt.% LS and 15 wt.% PSS, ground to the Blaine specific surface areas of 3500 cm^2/g. As seen, the general morphology of the microstructure of the hardened cement paste includes a matrix of hydration products in which portlandite crystals, partially reacted PSS particles, and a few clusters of agglomerated fine LS particles are embedded.

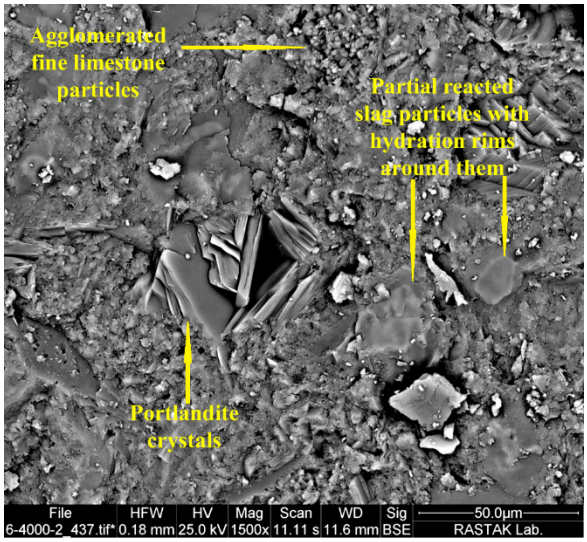

Fig. 15. SEM image of the 84-day cured paste of the selected ternary cement mix containing 15 wt.% limestones and 15 wt.% processed steel slag, ground to the Blaine fineness of 3500 cm^2/g.

Fig. 16 shows a typical SEM image of a cluster of fine LS agglomerated particles and the corresponding elemental profile obtained from EDAX elemental analysis performed on the selected area shown on the SEM image. As seen, the only element present in the analyzed area is calcium confirming the presence of calcite. The Au peaks correspond to the sample coating with Au for preparation for SEM.

Agglomeration and formation of clusters are the result of high fineness. Since LS is a much softer mineral than Portland cement clinker and PSS, it exhibits a significantly higher grindability in the intergrinding process compared to the other components [22], so that intergrinding of the mixtures can result in the formation of highly small LS particles tending to agglomerate and form clusters. This tendency increases at higher replacement levels [41].

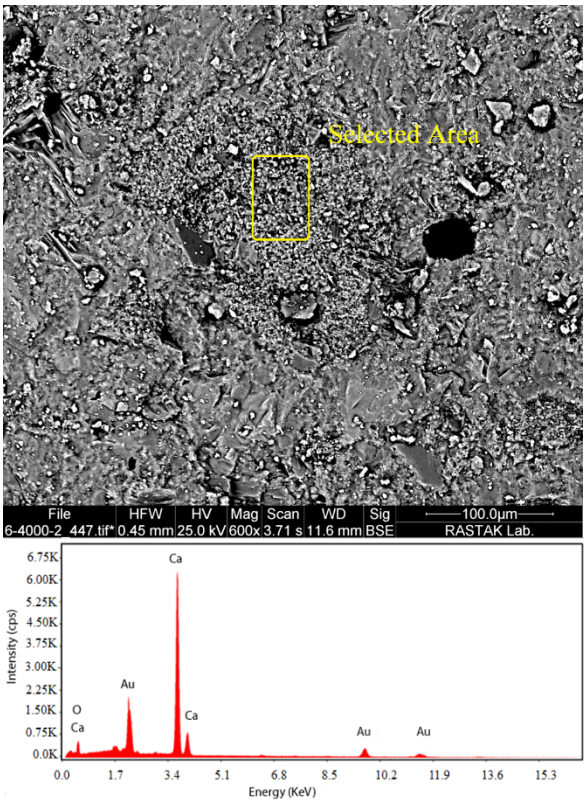

Fig. 16. A typical SEM image from a cluster of fine agglomerated limestone particles and the elemental profile obtained from EDAX analysis performed on the selected area.

Portlandite crystals exhibit column, hexagonal, and more frequently sheet morphology in hardened cement paste [42]. Observations by SEM confirmed a relatively high content of portlandite sheet crystals originated not only from the hydration of alite and belite phases of clinker, but also PSS (see Fig. 1). Fig. 17 shows a typical SEM image of a collection of sheet portlandite crystals embedded in the cement matrix and the elemental profile obtained from EDAX elemental analysis performed on the selected area shown on the SEM image.

As seen, the elemental profile displays calcium as the only element (except oxygen and hydrogen) present in the selected area. Fig. 18 shows a typical SEM image of a partially reacted PSS particle. As seen, the surface hydration of the PSS particle resulted in a well structural bonding to the cement matrix, and a color change from the PSS surface extended inwards confirming the formation of a

hydration reaction rim around the PSS particle. To track the changes happening during PSS hydration, EDAX analyses were performed on both hydration rim and non-reacted central part of PSS particle (the selected areas shown on SEM image).

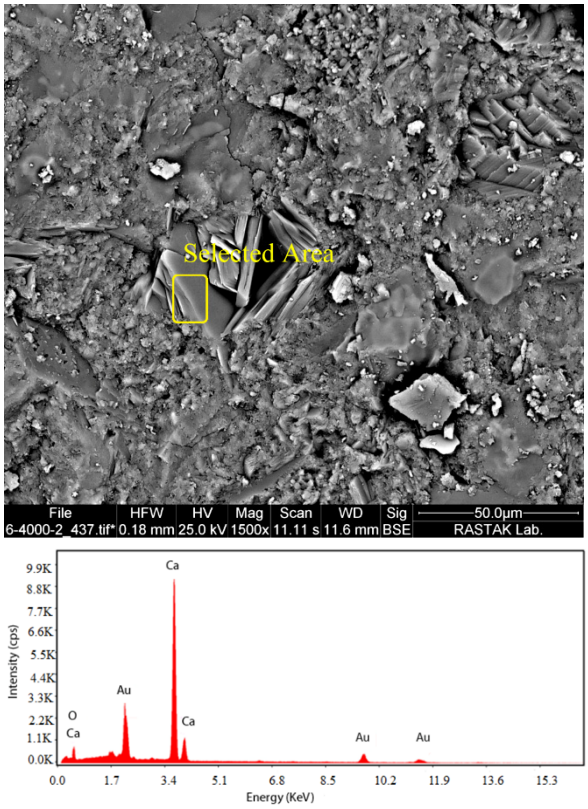

Fig. 17. A typical SEM image from a collection of portlandite crystals embedded in cement matrix and the elemental profile obtained from EDAX elemental analysis performed on the selected area.

Fig. 18 also shows the EDAX elemental profiles obtained from the selected areas.

Table 6 represents the elemental ratios between calcium, silicon, and aluminum as obtained by EDAX analyses for both hydration rim and non-reacted area of the PSS particle. Knowing that portlandite is the main crystalline phase of PSS, the decrease of Ca/Si ratio and the increase of Al/Si ratio in the hydration rim compared to the non-reacted part of the PSS particle could be attributed either to portlandite leaching from PSS particle and/or hydration progress of PSS hydraulic phases (mainly belite) releasing calcium hydroxide. The decrease in calcium content of the hydration rim enriches the aluminum content of which.

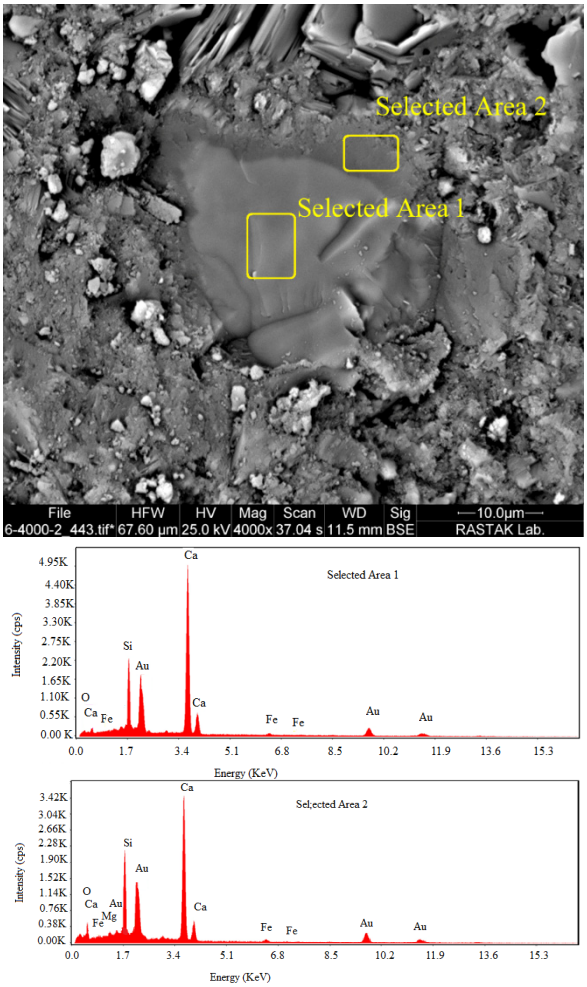

Fig. 18. SEM image from a partially reacted slag particle with a hydration rim around it.

Fig. 19. Ca/Si and Al/Si ratios in the non-reacted part and the reaction rim of the processed steel slag particle.

	Non-reacted slag	Slag hydration rim
Ca/Si	4.16	2.94
Al/Si	0.09	0.12

4. CONCLUSIONS

The importance of developing sustainable blended cements incorporating industrial wastes as supplementary cementing materials to consider industrial waste management, natural reserve conservation, and carbon dioxide emission reduction is well known. The present work evaluates the feasibility of processing and utilizing steel slag in binary and ternary cement blends with limestone. The achieved results confirm that processing steel slag by removing its

relatively high metallic content part not only increases its grindability for mechanical activation but also improves its hydraulic properties effectively and makes it suitable for being recycled in the cement industry.

The strength loss of the blended cement can be effectively compensated by mechanically activating the cement mixes to enhance the poor latent hydraulic properties of the processed steel slag. The results obtained show that despite the relatively low latent hydraulic property of the processed steel slag and almost non-reactivity of limestone, the physical and chemical characteristics of all the studied blended cement mixes comply with ASTM standard specifications, except the 28-day compressive strengths of the cement mixes containing 20 wt.% or higher amounts of limestone ground to the relatively low Blaine specific surface area of 3000 cm^2/g.

REFERENCE

[1] Menendez, G., Bonavetti, V. and Irassar, E. F., "Strength development of ternary blended cement with limestone filler and blast-furnace slag." Cem. Concr. Compos., 2003, 25, 61–67.

[2] Jianyong, L. and Pei, T., "Effect of slag and silica fume on mechanical properties of high strength concrete." Cem. Concr. Res., 1997, 27, 833–837.

[3] Bagel, L., "Strength and pore structure of ternary blended cement mortars containing blast-furnace slag and silica fume." Cem. Conc. Res., 1998, 28, 1011–1022.

[4] Thomas, M. D. A., Shehata, M. H., Shashiprakash, S. G., Hopkins, D. S. and Cail, K., "Use of ternary cementitious systems containing silica fume and fly ash in concrete." Cem. Conc. Res., 1999, 29, 1207–1214.

[5] Ozyildirim, C. and Halstead, W. J., "Improved concrete quality with combinations of fly ash and silica fume." ACI Mater. J., 1995, 91, 587–594.

[6] Virgalitte, S. J., Ehmke, B. A., Hooton, R. D., Lewis, D. W., Scali, M. J., Dhir, R. K. Idorn, G. M. and Malhotra, V. M., "Ground Granulated blast-furnace slag as a cementitious constituent in concrete." ACI Mater. J., 1987, 84, 321–342.

[7] U.S. Geological Survey, Mineral commodity summaries 2019, https://doi.org/10.3133/70202434

[8] U.S. Geological Survey, Mineral commodity summaries 2018, https://doi.org/10.3133/70194932

[9] Wang, Y. and Suraneni, P., "Experimental methods to determine the feasibility of steel slags as supplementary cementitious materials." Constr. Build. Mater., 2019, 204, 458-467.

[10] World Business Council for Sustainable Development and International Energy Agency, Cement Technology Roadmap 2009: Carbon Emissions Reductions up to 2050. https://www.wbcsd.org/Sector-Projects/Cement-Sustainability-Initiative/News/ (2009).

[11] Cao, L., Shen, W., Huang, J., Yang, Y., Zhang, D., Huang, X., Lv, Z. and Ji, X., "Process to utilize crushed steel slag in cement industry directly: Multiphased clinker sintering technology." J. Clean. Prod., 2019, 2017, 520-529.

[12] Jiang, Y., Ling, T. C., Shi, C. and Pan, S. Y., "Characteristics of steel slags and their use in cement and concrete— A review." Resour. Conserv. Recycl., 2018, 138, 187-197.

[13] Alanyali, H., Çöl, M., Yilmaz, M. and Karagöz, Ş., "Concrete produced by steel-making slag (basic oxygen furnace) addition in Portland cement." Int. J. Appl. Ceram. Technol., 2009, 6, 736–748.

[14] Shi, C., "Steel slag-its production, processing, characteristics, and cementitious properties." J. Mater. Civ. Eng., 2004, 16, 230–236.

[15] Proske, T., Hainer, S., Rezvani, M. and Graubner, C. A., "Eco-friendly concretes with reduced water and cement contents— Mix design principles and laboratory tests." Cem. Concr. Res., 2013, 51, 38–46.

[16] Palm, S., Proske, T., Rezvani, M., Hainer, S., Müller, C. and Graubner, C.-A., "Cements with a high limestone content– Mechanical properties, durability and ecological characteristics of the concrete." Constr. Build. Mater., 2016, 119, 308–318.

[17] Voglis, N., Kakali, G., Chaniotakis, E. and Tsivilis, S., "Portland-limestone cements. Their properties and hydration compared to

those of other blended cements." Cem. Concr. Compos., 2005, 27, 191–196.
[18] Vuk, T., Tinta, V., Gabrovšek, R. and Kaučič, V., "The effects of limestone addition, clinker type and fineness on properties of Portland cement." Cem. Concr. Res., 2001, 31, 135–139.
[19] Lothenbach, B., Le Saout, G., Gallucci, E. and Scrivener, K., "Influence of limestone on the hydration of Portland cements." Cem. Concr. Res., 2008, 38, 848–860.
[20] Bonavetti, V., Rahhal, V. and Irassar, E., "Studies on the carboaluminate formation in limestone filler-blended cements." Cem. Concr. Res., 2001, 38, 853–859.
[21] Proske, T., Rezvani, M., Palm, S., Müller, C. and Graubner, C.-A., "Concretes made of efficient multi-blended cements with slag and limestone." Cem. Concr. Compos., 2018, 89, 107-119.
[22] Ghiasvand, E. and Ramezanianpour, A. A., "Effect of grinding method and particle size distribution on long term properties of binary and ternary cements." Constr. Build. Mater., 2017, 134, 75–82.
[23] Behim, M., Beddar, M. and Clastres, P., "Reactivity of granulated blast furnace slag." Slovak j. civ. Eng., 2013, XXI, 7–14.
[24] Kourounis, S., Tsivilis, S., Tsakiridis, P.E., Papadimitriou, G.D. and Tsibouki, Z., "Properties and hydration of blended cements with steelmaking slag." Cem. Concr. Res., 2007, 37, 815–822.
[25] Voglis, N., Kakali, G., Chaniotakis, E. and Tsivilis, S., "Portland-limestone cements. Their properties and hydration compared to those of other blended cements." Cem. Concr. Compos., 2005, 27, 191-196.
[26] Allahverdi, A. and salem, S., "Simultaneous influences of microsilica and limestone powder on properties of portland cement paste, Ceram. Silic., 2010, 54, 65-71.
[27] Black, L., sustainability of construction materials, second ed., 2016.
[28] Allahverdi, A. and Ahmadnezhad, S., "Mechanical activation of silicomanganese slag and its influence on the properties of Portland slag cement." Powder Technol., 2014, 251, 41–51.
[29] Qian, Y., Chengjin, S., Shu, S., Rui, C. and Hongjian, S., "The sulfate corrosion resistance behavior of slag cement mortar." Constr. Build. Mater., 2014, 71, 202–209.
[30] Ogawa, S., Nozaki, T., Yamada, K., Hirao, H. and Hooton, R. D., "Improvement on sulfate resistance of blended cement with high alumina slag." Cem. Concr. Res., 2012, 42, 244–251.
[31] kucharczyk, S., Zajac, M. and Deja, J., "The influence of limestone and Al_2O_3 content in the slag on the performance of the blended cements." Procedia Eng., 2015, 108, 402-409.
[32] Ghorbel, H. and Samet, B., "Effect of iron on pozzolanic activity of kaolin." Constr. Build. Mater., 2013, 44, 185-91.
[33] Grilo, J., Santos, S. A., Faria, P., Gameiro, A., Veiga, R. and Velosa, A., "Mechanical and mineralogical properties of natural hydraulic lime-metakaolin mortars in different curing conditions." Constr. Build. Mater., 2014, 51, 287-294.
[34] Ylmén, R., Jäglid, U., Steenari, B. M. and Panas, I., "Early hydration and setting of Portland cement monitored by IR, SEM and Vicat techniques." Cem. Concr. Res., 2009, 39, 433–439.
[35] Sáez del Bosque, I. F., Martínez-Ramírez, S. and Blanco-Varela, M.T., "FTIR study of the effect of temperature and nanosilica on the nano structure of C–S–H gel formed by hydrating tricalcium silicate." Constr. Build. Mater., 2014, 52, 314–323.
[36] Yu, P., Kirkpatrick, R. J., Poe, B., McMillan, P.F. and Cong, X., "Structure of calcium silicate hydrate (C–S–H): near-, mid-, and far-infrared spectroscopy." J. Am. Ceram. Soc., 1999, 82, 742–748.
[37] Silva, D. A., Roman, H. R. and Gleize, P.J.P., "Evidences of chemical interaction between EVA and hydrating Portland cement." Cem. Concr. Res., 2002, 32, 1383–1390.
[38] Richard, T., Mercury, L., Poulet, F. and d'Hendecourt, L., "Diffuse reflectance infrared Fourier transform spectroscopy as a tool to characterise water in adsorption/ confinement situations." J. Colloid. Interface. Sci., 2006, 304, 125–136.
[39] Mollah, M.Y.A., Schennach, W. Yu, R. and Cocke, D.L., "A Fourier transform infrared spectroscopic investigation of the

early hydration of Portland cement and the influence of sodium lignosulfonate." Cem. Concr. Res., 2000, 30, 267–273.

[40] Trezza, M. A. and Lavat, A. E., "Analysis of the system $3CaO \cdot Al_2O_3 - CaSO_4 \cdot 2H_2O - CaCO_3 - H_2O$ by FT-IR spectroscopy." Cem. Concr. Res., 2001, 31, 869–872.

[41] Knop, Y., Peled, A. and Cohen, R., "Influences of limestone particle size distributions and contents on blended cement properties." Constr. Build. Mater., 2014, 71, 26–34.

[42] Franus, W., Panek, R., Wdowin, M. and et al., SEM investigation of microstructures in hydration products of Portland cement, in: E.K. Polychroniadis (Ed.), 2nd International Multidisciplinary Microscopy and Microanalysis Congress, Springer International Publishing, Switzerland, 2015, 105–112.